Complex Rotating Waves and Long Transients in a Ring Network of Electrochemical Oscillators with Sparse Random Cross-Connections

Michael Sebek,[1] Ralf Tönjes,[2] and István Z. Kiss[1]
[1]Department of Chemistry, Saint Louis University, 3501 Laclede Avenue, St. Louis, Missouri 63103, USA
[2]Institute of Physics and Astronomy, Potsdam University, 14476 Potsdam-Golm, Germany
(Received 14 July 2015; published 11 February 2016)

We perform experiments and phase model simulations with a ring network of oscillatory electrochemical reactions to explore the effect of random connections and nonisochronicity of the interactions on the pattern formation. A few additional links facilitate the emergence of the fully synchronized state. With larger nonisochronicity, complex rotating waves or persistent irregular phase dynamics can derail the convergence to global synchronization. The observed long transients of irregular phase dynamics exemplify the possibility of a sudden onset of hypersynchronous behavior without any external stimulus or network reorganization.

DOI: 10.1103/PhysRevLett.116.068701

Wave propagation of activity of oscillatory units in rings or linear chains is a fundamental type of pattern formation that occurs in many biological systems, e.g., the motion of a leach [1], the segmentation clock [2], or brain wave activities in the cortex [3]. A rotating pinwheel was one of the first types of chemical pattern formation identified in the Belousov-Zhabotinsky (BZ) reaction on a ring [4]. As a ring geometry is often used in chemistry, rotating phase wave patterns have been observed in a large number of systems, e.g., in electrochemical reactions [5], heterogeneous catalysis [6], coupled BZ reactors [7], and microdroplets [8]. Mathematical analysis using phase models interpreted the existence and local stability of rotating waves in ring networks [9–11]. It was found that the fully synchronized, zero phase lag, nonrotating state is the most attracting solution, locally and globally. However, with increasing system size, rotating waves with higher winding number become more probable in the aggregate [12].

Complex engineered and biological systems can often be described as networks of discrete, interacting units [13]. Considering the prevalence of phase waves on rings and chains, a fundamental question is how the rotating waves manifest in networks that are composed of a regular ring backbone with a few additional random connections. Numerical simulations with phase models on sparse directed networks with random initial phases have shown that for sufficiently nonisochronous oscillations, while the fully synchronized state is locally stable, persistent irregular phase dynamics is the typically observed behavior [14]. Such prolonged transient behavior can severely impact system response when robust synchronization is required, as it was demonstrated with power grid models [15] or when synchronization is undesirable, e.g., in hypersynchronous neuronal discharges during seizures [16].

In this Letter, we explore the type of spatiotemporal patterns that can be obtained with oscillatory chemical reactions on bidirectional ring networks with random long-range connections. The experimental work is motivated by phase model calculations that predict the presence of complex rotating waves and long transients in small random networks with sufficiently nonisochronous oscillations. The experimental conditions allow the analysis of the dependence of pattern formation on the randomness of the network topology and the level of nonisochronicity of the interactions among the units.

To study the properties of complex rotating waves on networks we consider weakly coupled, identical limit cycle oscillators with a Kuramoto type phase model [17] for phase differences in a corotating frame of reference

$$\dot{\vartheta}_n = \sum_{m=1}^{N} A_{nm} g(\vartheta_m - \vartheta_n), \tag{1}$$

where A_{nm} represents a coupling matrix and $g(\Delta\vartheta)$ is the average effect of the coupling for oscillators with phase difference $\Delta\vartheta$. A phase attractive coupling is assumed with interaction function $g(\Delta\vartheta) = \sin(\Delta\vartheta - \alpha) + \sin(\alpha)$. The phase shift parameter α is an important system property determined by the average shear flow near the limit cycle in the direction of perturbation caused by coupling [17]; i.e., α quantifies the nonisochronicity of the oscillations induced by interactions. We note that since the dynamics of the model equations [Eq. (1)] is invariant under a change of $\alpha \to -\alpha$, $\vartheta \to -\vartheta$, and $t \to -t$, the phase differences and the frequency shift are inverted when α changes sign, such that sources become sinks of rotating waves and vice versa. We assume non-normalized, bidirectional coupling $A_{mn} = A_{nm} \in \{0, 1\}$ on ring networks of $N = 500$ oscillators with $N_{sc} = \sigma N$ additional random bidirectional links. The initial conditions for the simulations and the experiments is a rotating wave on the ring. (Random initial conditions give comparable results.)

Because of phase attractive coupling $g'(0) = \cos\alpha > 0$ and the complete connectedness of the network, the fully synchronized, one-cluster state is always a linearly stable solution of Eq. (1) [14]. However, the typical behavior of the network starting from globally desynchronized initial conditions, is far more complex than the intuitively expected relaxation to the one-cluster state. We characterize the state of the system by different order parameters. The k-cluster order parameters $R_k = \langle \exp(ik\vartheta_n) \rangle$, where the average is taken instantaneously over all oscillators, measure the coherence of the distribution of phases into k evenly spaced clusters. The variance $\mathrm{var}\dot{\vartheta}$ of the phase velocities is a measure for frequency synchronization. These ensemble averaged measures are shown in the σ vs α parameter plane in Figs. 1(a) and 1(b).

With small σ, the original ring is divided into linear segments between the end points of shortcuts, which can support traveling phase waves. At the interfaces where two such traveling waves meet, the phase differences in a state of stable synchronization are restricted. At low nonisochronicity and low shortcut density these interfaces can be frozen when all topological boundary conditions can be met simultaneously. We refer to such a pattern, which does not change in time, as a frozen complex rotating wave pattern. When the topological boundary conditions are not met (this is likely to occur with a large number of oscillators), slowly changing interfaces are obtained, reminiscent of vortex glasses in 2D oscillatory media [18]. Both the Kuramoto order parameter R_1 and the variance of the phase velocities are small in this regime. When the shortcut density is increased, there exists a topological crossover to a random network without linear chain segments. Therefore, when σ is increased the system cannot maintain rotating waves and the one-cluster state becomes globally attractive with $R_1 \approx 1$. When α is increased from zero, higher shortcut densities are required for complete synchronization [Figs. 1(a)–1(c)].

At large values of nonisochronicity ($\alpha \gtrsim 1$) a qualitatively different type of behavior exists. The topological boundary conditions for rotating phase waves along the ring segments with stationary phase differences are very difficult to satisfy simultaneously. Instead, the dominant behavior is persistent irregular dynamics with nonzero $\mathrm{var}\dot{\vartheta}$. The distribution of phase differences during the transient and in frozen complex rotating patterns becomes bimodal, suggesting a preferred phase difference that depends on α [Fig. 2(b)]. The emergence of persistent irregular dynamics is demonstrated in Fig. 1(d) by fixing the shortcut density σ, and increasing the value of α. At the transition between frozen and unfrozen complex rotating patterns, global clustering can arise resulting in a sharp increase in the order parameters R_6 or R_7. This global order is mediated by the end points of the shortcuts in the network [Fig. 2(f)] Because of the narrow distribution of phase differences in a phase locked state, oscillators at the same distance to a cross-linked node have the same phase. Global clustering is only observable in a narrow parameter region at criticality and after a long, system size dependent transient.

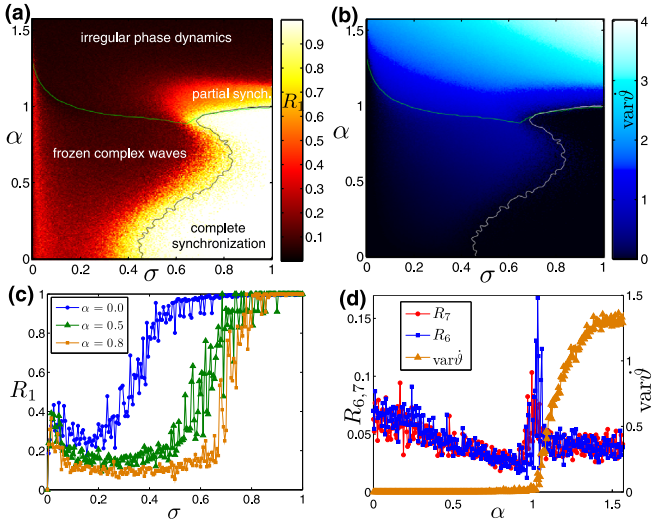

FIG. 1. Order parameters in model (1) at time $t = 500$ as functions of shortcut density σ and nonisochronicity parameter α averaged over ten random network realizations with $N = 500$ oscillators and rotating wave initial conditions. (a) Color coded Kuramoto order parameter R_1 and (b) variance $\mathrm{var}\dot{\vartheta}$ of phase velocities. The black and the white lines in (a) and (b), respectively, mark the contour of $R_1 = 0.9$. The light (green) line marks the contour line of $\mathrm{var}\dot{\vartheta} = 0.2$. (c) Kuramoto order parameter as a function of σ for three different values of α [cf. Fig. 3(c)]. (d) Mean cluster order parameters R_6, R_7, and variance of phase velocities as functions of α at $\sigma = 0.15$.

In addition, around the transition point, before a complex rotating wave pattern becomes frozen, very long transient dynamics can be observed. Figure 2 shows an example of such transient dynamics, from random initial conditions and with negative nonisochronicity. The time evolution of next-neighbor phase differences demonstrates the competition between different phase patterns, with stationary sinks of the phase waves located at the network heterogeneities and dynamically rearranging sources which may form or annihilate upon collision with a sink or at phase slip events. Figures 2(d) and 2(e) show a transient and a stationary phase profile, respectively, and Fig. 2(b) illustrates the time evolution of the phase difference distribution. The phase differences in the stationary phase pattern are peaked sharply around $2\pi/7$ resulting in a very precise wavelength and the formation of 7 global phase clusters. As shown in Fig. 1(a), there also exists a narrow regime of partial synchronization for larger shortcut densities, which is replaced in a sharp discontinuous transition by persistent incoherent phase dynamics at values of α approaching $\pi/2$ and which may be analyzed in a mean field approach [19].

To confirm the modeling results, experiments were performed with an array of $N = 20$, 1.00 mm diameter

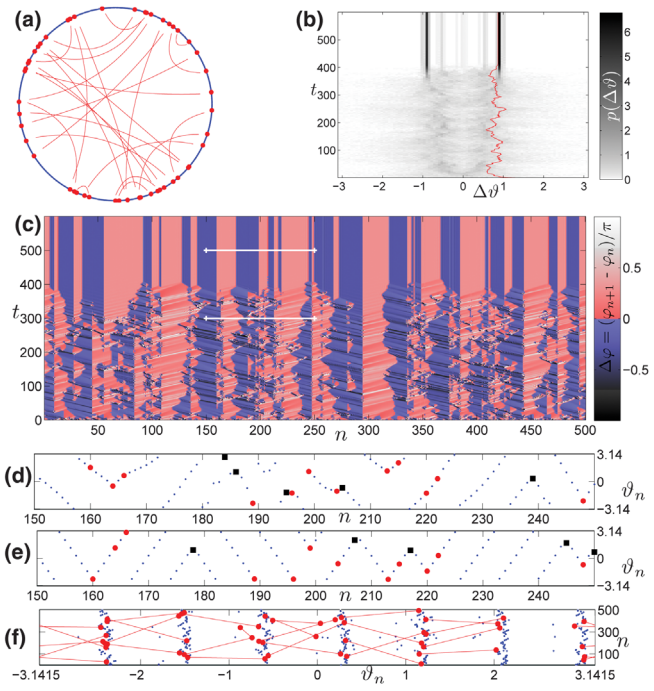

FIG. 2. Long transient to a complex frozen rotating wave pattern from random initial phases in a network of $N = 500$ phase oscillators with $\alpha = -1.15$ and shortcut density $\sigma = 0.05$. (a) Ring network with 26 additional random shortcuts. (b) Time evolution of the density of next neighbor phase differences. The solid (red) line marks the average of $|\Delta\vartheta|$. (c) Time evolution of next neighbor phase differences modulus π (color coded). Dark (blue) colors indicate phase waves to the right and light (red) colors indicate phase waves to the left. The white lines indicate phase profiles ϑ_n between $150 \leq n \leq 250$ shown in (d) at $t = 300$ and (e) at $t = 500$. Large (red) circles and solid (red) lines in panels (a),(d)–(f) indicate nodes with shortcut connections. Black squares in panels (d),(e) indicate dynamically realized centers of phase waves. Panel (f) shows clustering of the phases at $t = 500$ with $R_7 \approx 0.9$ and cross-links (solid lines) connecting neighboring clusters.

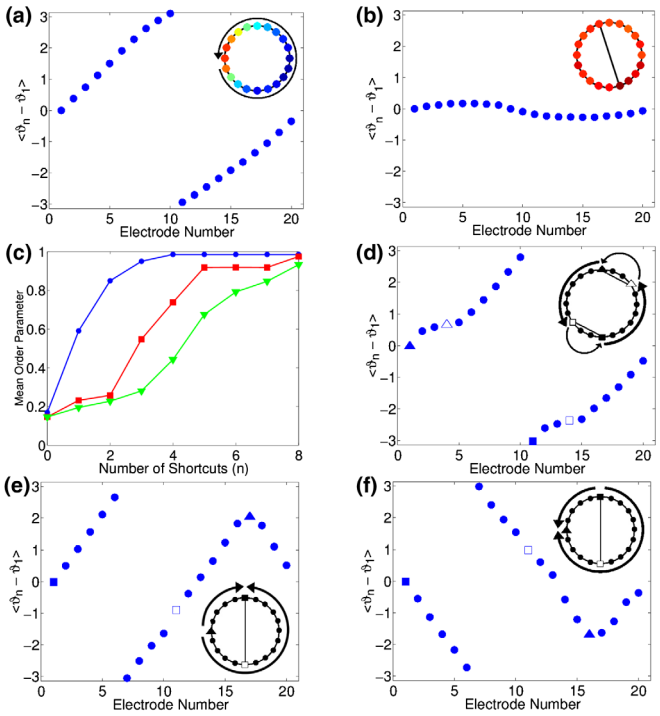

FIG. 3. The impact of shortcuts and α on the formation of complex rotating waves and on synchronization. (a) Initial rotating wave ($V = 1105$ mV, $K = 0.20$ mS, $\alpha = 0$). (b) Synchrony induced by one long-distance shortcut. (c) The mean order parameter with increasing number of shortcuts at $\alpha = 0$ (circles), -0.97 (squares), and -1.3 (triangles). $V = 1110$ mV, $C_c = 82$ μF, $K = 0.10$ mS at $\alpha = -0.97$ and $K = 0.025$ mS at $\alpha = -1.3$. (d) Short distance shortcuts at $\alpha = 0$ yield jumping waves ($V = 1110$ mV). (e) Long distance shortcut at $\alpha = -0.97$ yields a frozen complex rotating pattern with a source (triangle) away from the heterogeneity ($V = 1110$ mV). (f) Long distance shortcut at $\alpha = 0.76$ yields a frozen complex rotating pattern with a source (full square) on the heterogeneity ($V = 1245$ mV, $C_{\text{ind}} = 1$ mF, $K = 0.40$ mS).

nickel wires on which an oscillatory metal dissolution reaction takes place measured by currents. Numerical simulations indicate (see Supplemental Material [20], which includes Ref. [21]) that regions of frozen rotating patterns, complete synchronization, and irregular phase dynamics can be clearly distinguished even in such a small setup. The electrodes are coupled into a ring topology with additional random cross-connection via resistances and capacitances. We report the conductance across the coupling resistance as coupling strength K. Capacitance is used to introduce nonisochronicity through a phase shift in the coupling current [20,21]. The initial condition of the experiment is a rotating wave as shown in Fig. 3(a). First, we describe the results with $\alpha = 0$, i.e., resistive coupling. When a random cross-connection was added, one of two scenarios occurred. If the random shortcut connected two elements at a distance larger than 4 units, the system quickly converged to a fully synchronized state similar to that shown in Fig. 3(b). When the distance between the shortcut elements was smaller, the rotating waves jumped across the connection. Figure 3(d) shows such a pattern with two cross-connections.

We have performed 16 independent trials adding cross-connections successively to a ring configuration. The mean order parameter as a function of the added number of shortcuts is shown in Fig. 3(c). Only three shortcuts were required for the average order parameter to exceed 0.90. Therefore, we can conclude that with $\alpha = 0$ a relatively small number of shortcuts ($\sigma \approx 0.15$) induces full synchrony. When α was changed to -0.97, with a parallel RC coupling, we still observed rotating waves jumping over the connection when the first cross-connection was placed up to a distance of 5 units between the elements. However, when the distance was larger, instead of full synchronization, we observed a frozen complex rotating pattern via the formation of a source and sink pair [Fig. 3(e)]. The order parameter vs number of shortcuts graph in Fig. 3(c) shows

that with $\alpha = -0.97$ the mean order parameter starts to increase for $n > 3$, and it requires a relatively large number ($n > 6$) of random shortcuts to achieve Kuramoto order larger than 0.90. The presence of jumping waves and complex rotating wave patterns thus contributes to resisting complete synchronization. When α was further changed to -1.3, the trend of resisting the fully synchronized state continued. Figures 3(e) and 3(f) demonstrate the inversion of the stationary phase profile, and thus the direction of the rotating waves and the reversal of source and sink, upon switching the sign of the nonisochronicity by adding a capacitance to the individual current instead of the coupling current [20,21]. All the patterns in Fig. 3 were reproduced by phase model simulations in the Supplemental Material [20]. Long transients to both frozen complex wave patterns and identical synchronization were observed in experiment. A long transient over 1700 s in a network with five random shortcuts near $\alpha = -1.3$ is shown in Fig. 4. The time evolution of next neighbor phase differences during the transient is shown in Fig. 4(a). At least two competing wave patterns, which are metastable over the course of tens of oscillations and transform via intermittent phase slips could be observed for over 700 oscillations before the system settled into the one-cluster state. At $\alpha = 0$ the same network relaxes exponentially to synchronization in 230 s [20]. Numerical simulations with the phase model

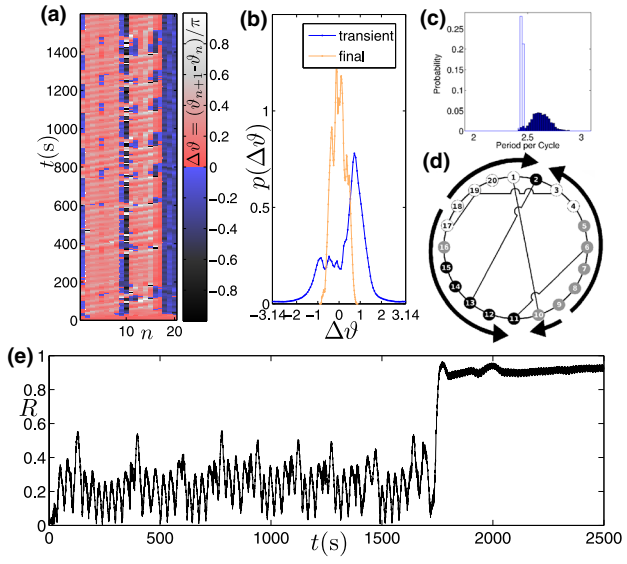

FIG. 4. Long transient to synchronization at $\alpha = -1.3$ ($V = 1110$ mV, $C_c = 82$ μF, $K = 0.033$ mS). (a) Time evolution of next neighbor phase differences. (b) Histogram of next neighbor phase differences during the transient and the final synchronized state. (c) Histogram of the period per cycle of all electrodes (white bars are the individual periods and dark bars the transient). (d) Network topology and a typical complex rotating wave pattern during the transient. Arrows indicate the wave direction from sources to sinks. (e) Time evolution of the Kuramoto order parameter where the arrows indicate transitions between wave patterns through phase slips.

confirmed that by changing α from 0 to -1.3 the lifetime of the transient increases about 10 times and diverges as α approaches $|\pi/2|$ [20]. A density plot of next neighbor phase differences during and after the transient is depicted in Fig. 4(b) and shows an asymmetric distribution with a preferred wavelength, skewed towards the initial left-handed rotational state. In addition, a wide distribution of peak-to-peak periods can be observed during the transient as seen in Fig. 4(c), which marks the presence of irregular phase dynamics. A typical snapshot of a transient complex rotating wave is shown in Fig. 4(d). The arrows indicate the direction of the rotations as well as the sources (oscillators 9 and 18) and sinks (oscillators 2 and 11) of the unstable rotational wave pattern. The order parameter [Fig. 4(e)] clearly exhibits the transient behavior as its value changes between approximately 0.2 and 0.6 irregularly throughout the transient until synchronization is achieved.

In conclusion, we have observed frozen complex rotating patterns and long transients to synchronization in electrochemical oscillations and numerical simulations of phase oscillators on a ring network topology with sparse random shortcuts. Depending on the sign of nonisochronicity α, either the sinks or the sources are pinned to end points of cross-connections in the network. At increased nonisochronicity the variability in the phase differences in a phase locked state decreases until synchronization is no longer possible and persistent, or very long transient phase dynamics occurs. The presence of long transients of irregular phase dynamics could have relevance in the functioning of biological systems, e.g., in neuron dynamics where pathological synchronization can occur without apparent external perturbation or change of network topology. The experimentally recorded, irregular transient dynamics contributes to the few experimental examples of high dimensional transient chaos [22], where system size effects on the lifetime of the transient irregular state could be studied.

This material is based upon work supported by the National Science Foundation under Grant No. CHE-1465013.

[1] T. Iwasaki, J. Chen, and W. O. Friesen, Proc. Natl. Acad. Sci. U.S.A. **111**, 978 (2014).
[2] V. M. Lauschke, C. D. Tsiairis, P. Francois, and A. Aulehla, Nature (London) **493**, 101 (2012).
[3] G. Ermentrout and D. Kleinfeld, Neuron **29**, 33 (2001).
[4] Z. Noszticzius, W. Horsthemke, W. D. McCormick, H. L. Swinney, and W. Y. Tam, Nature (London) **329**, 619 (1987).
[5] H. Varela, C. Beta, A. Bonnefont, and K. Krischer, Phys. Chem. Chem. Phys. **7**, 2429 (2005).
[6] D. Luss and M. Sheintuch, Catalysis Today **105**, 254 (2005).
[7] J. P. Laplante and T. Erneux, J. Phys. Chem. **96**, 4931 (1992).

[8] N. Tompkins, N. Li, C. Girabawe, M. Heymann, G. B. Ermentrout, I. R. Epstein, and S. Fraden, Proc. Natl. Acad. Sci. U.S.A. **111**, 4397 (2014).
[9] G. Ermentrout, J. Math. Biol. **23**, 55 (1985).
[10] G. B. Ermentrout, SIAM J. Appl. Math. **52**, 1665 (1992).
[11] N. Kopell and G. Ermentrout, Commun. Pure Appl. Math. **39**, 623 (1986).
[12] D. A. Wiley, S. H. Strogatz, and M. Girvan, Chaos **16**, 015103 (2006).
[13] R. Albert and A. L. Barabasi, Rev. Mod. Phys. **74**, 47 (2002).
[14] R. Toenjes, N. Masuda, and H. Kori, Chaos **20**, 033108 (2010).
[15] P. J. Menck, J. Heitzig, J. Kurths, and H. Joachim Schellnhuber, Nat. Commun. **5**, 3969 (2014).
[16] P. J. Uhlhaas and W. Singer, Neuron **52**, 155 (2006).
[17] Y. Kuramoto, *Chemical Oscillations, Waves and Turbulence* (Springer, Berlin, 1984).
[18] C. Brito, I. S. Aranson, and H. Chaté, Phys. Rev. Lett. **90**, 068301 (2003).
[19] T.-W. Ko and G. B. Ermentrout, Phys. Rev. E **78**, 016203 (2008).
[20] See Supplemental Material at http://link.aps.org/supplemental/10.1103/PhysRevLett.116.068701 for Experimental setup and method, and comparison to phase simulations with $N = 20$ oscillators..
[21] M. Wickramasinghe and I. Z. Kiss, Phys. Rev. E **88**, 062911 (2013).
[22] T. Tamás and Y.-C. Lai, Phys. Rep. **460**, 245 (2008).